Fast Walking with Rhythmic Sway of Torso in A 2D Passive Ankle Walker

Ruizhi Bao Tao Geng

***Abstract* —There is a category of biped robots that are equipped with passive or un-actuated ankles, which we call Passive-Ankle Walkers (PAWs). Lack of actuation at ankles is a disadvantage in the fast walking of PAWs. We started this study with an intuitive hypothesis that rhythmic sway of torso may enable faster walking in PAWs. To test this hypothesis, firstly, we optimized the rhythmic sway of torso of a simulated PAW model for fast walking speed, and analyzed the robustness of the optimal trajectories. Then we implemented the optimal trajectories on a real robot. Both the simulation analysis and the experimental results indicated that optimized torso-swaying can greatly increase the walking speed by 40%. By analyzing the walking patterns of the simulated model and the real robot, we identified the reason for the faster walking with swaying-torso: The rhythmic sway of torso enables the robot to walk with a relatively large step-length while still keeping a high step-frequency.**

***Index Terms*— Biped robots, legged locomotion.**

I. Introduction

In human walking, the ankle of the stance leg pushes off at the end of the stance phase. This powerful push-off adds net work in each walk step to offset the energy loss caused by the heel-striking of the swing leg [1][2]. Hobbolen and Wisse studied a simulation model and a prototype biped robot, and found that ankle push-off can increase the walking speed effectively [3]. Dean and Kuo's simulation analysis of a biped model indicated that the overall walking speed increases roughly with the square root of this push-off magnitude [4]. So, the ankle push-off plays a critical role in the fast walking of human and biped robots.

However, not all walking robots can employ ankle push-off for their fast walking. There is a category of biped robots whose ankle joints or feet are not actuated. Here we call them Passive Ankle Walkers (PAWs). Most of the PAWs are equipped with pointed or curved feet and are planar bipeds [5][6][7][8][9]. These planar biped robots are used to study the forward movement of the robot in the sagittal plane. Their movements are constrained in the sagittal plane usually by a boom structure. The lack of actuation at the ankles of PAWs is a disadvantage in their fast walking. Fig. 1 illustrates the movement of the robot torso during the stance phase of a passive-ankle walker. During the first half of the stance phase (form A to B in Fig. 1), the robot torso moves like an inverted pendulum that is climbing up to its apex using only its inertia, and thus the speed of the Centre of Mass (CoM) is decreasing from A to B, which we call "the braking phase". During the second half of the stance phase (from B to C in Fig. 1), the robot is falling down and its speed of the CoM is increasing, which we call "the accelerating phase".

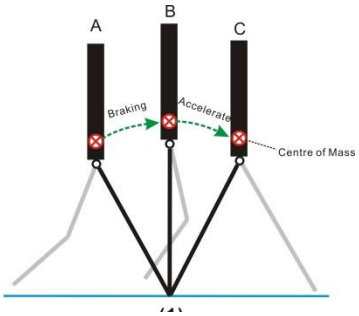

Fig.1 Illustrations of the braking-and-accelerating effect in PAW's walking.

If we want a PAW to walk fast, we must attenuate the drastic braking-and-accelerating effect. To achieve this, we propose a new strategy in this study: Optimizing the rhythmic say of a high torso to facilitate fast biped walking.

In most of the biped/humanoid robots (including the robot in this study), a large proportion of the mass is located at the torso. Therefore, the movement and pose of the torso can fundamentally influence the dynamics of the walking gait. Unlike in many other biped/humanoid robots that keep their torsos upright stably, the torso of our robot is allowed to sway forward and backward. If being optimized properly, this rhythmic sway of the torso might somewhat compensate the braking-and-accelerating effect in PAWs. Thus, the braking-and-accelerating effect might be mitigated by rhythmic sway of the torso. We postulate that the proposed strategy might enable the PAW to walk with a large step-length while still keeping a high step-frequency. In this way, the PAW's walking speed may be increased greatly.

Of course, it's not new to study the movement of the torso in biped robots. How the mass distribution and movement of the torso could affect various aspects of biped walking have been studied in-depth in the literature. Some studies have analyzed the effects of torso (or upper body) on the stability [11] [12] [13] [14] [15], robustness [15] [16], energy efficiency [13] [15], and motion smoothness [17] of biped walking robots. A few other studies have also considered how to exploit the torso movement to improve the performance of humanoid/biped robots. For example, Ugurlu *et al* used torso rotation in the ground plane to compensate the undesired yaw motion of a humanoid robot [18]. Kang *et*

This research was funded by the EPSRC in the UK (EP/P00542X/1). R. Bao is with Brunel University, London, UK (email: rzbao1993@gmail.com). T. Geng is with Middlesex University, London, UK (e-mail: runbot05@gmail.com). .

al optimized the torso motion to compensate the deviation from the ZMP stability criterion in a biped robot [19]. Dallali *et al* designed a ZMP feedback controller that utilizes the upper body to balance the humanoid robot [20]. Kappaganthu *et al* designed a novel half-passive biped. Only its torso is actuated and all other joints are passive [21]. They optimized the torso movement in terms of energy cost, to drive the robot's stable walking.

However, how the rhythmic sway of torso could affect the walking speed of biped robots has not been analyzed in the literature.

Grizzles' group has found that the walking speed of planar biped robots could be increased by simply leaning its torso forward at a fixed angle [6][25]. In this study we consider a more dynamic movement of the torso – rhythmically swaying forward and backward during a gait cycle. We ask us this question: Can this rhythmic sway of torso increase the walking speed of passive ankle walkers? If it can, what is the reason?

The rest of the paper is organized as follows. In Section II, we briefly describe the mechanical design and the controller of the robot. Section III presents the dynamics model of the robot and the optimization process. Section IV analyzes the walking speed and robustness of the optimal walking patterns. The experimental results of the prototype robot are summarized in Section V. Finally, Section VI concludes the paper by pointing out the drawbacks of the proposed strategy.

II. THE ROBOT AND ITS CONTROLLER

A. *Mechanical structure of the robot*

The actuators, the sensors, and the leg-length of the robot are similar to that of another robot designed in our previous study [7]. However, there is one fundamental difference between them: In order to investigate the effects of the torso on walking speed, the robot in this study is equipped with a much higher torso, which makes the robot's total weight twice larger than that of our previous design. Due to this heavy and high torso (see Fig. 2), the dynamics of the robot is critically changed and becomes more complex. The new robot would not be able to walk fast with the controller of our previous study in [7]. The robot is shown in Fig. 2. For its details, please see [33].

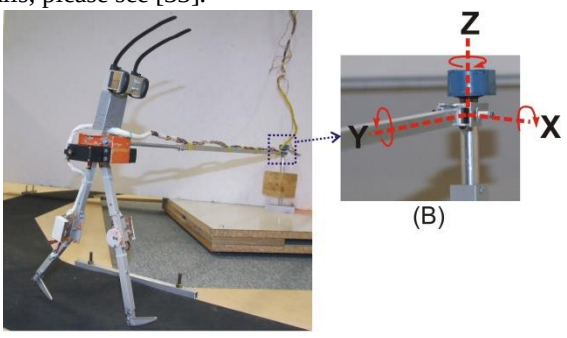

Fig. 2 The robot (A), and its boom structure (B). The encoder for measuring the walking speed is installed at the Z axis of the boom.

B. *The controller*

Each leg of the robot has two phases: stance phase and swing phase. At each joint, there is a PD controller to drive the joint to track the planned trajectory. At the inter-leg level and the step-to-step level, there is a simple state machine that switches the phases of each leg whenever the swing leg lands [33]. This kind of event-based step-to-step control or phase-resetting can stabilize the walking gait of the real robot even when the planned or desired trajectories are not stable. In this study, because the desired trajectories obtained in the optimization of a simulated model will be implemented on the real robot, un-modeled dynamics and inevitable disturbances in real system could undermine the stability. This step-to-step control will be very helpful to the stability and robustness of the real robot. The desired trajectories of the stance phase and swing phase will be defined by the optimization process in the next section.

III. OPTIMIZATION PROCESS

In this section, we first construct the trajectories of the robot movement with polynomial functions and the dynamics model. Then we optimize the trajectories in terms of walking speed. The optimization method used in this study is an nonlinear constrained optimization algorithm, which were popularly applied on the trajectory planning of biped walking robots [5][6][32][29]. The method will be briefly described in sub-section III.B. Details of this method is available in [32].

A. *Constructing the joint trajectories*

The kinematics model of the planar biped robot used in the simulation is shown in Fig. 3. The mechanical structure, the size and mass of each link, and the controller are the same as that of the real robot described in the previous section. The frictions at joints are ignored and the duration of double support phase is assumed to be infinitesimal. The biped robot is a hybrid dynamic system involving three stages in each gait cycle:

(1) Single support stage: one foot is on the floor while the other foot is swing forward. The system is in a continuous state during this phase.

(2) Landing stage: when the swing heel lands, it has impact with the floor. This is a discrete transient phase.

(3) Double support stage: both feet are on the floor. Following many other studies on the simulation of passive-ankle walker [3][4][5][6][7][9], this transient stage is assumed to be instantaneous and takes no time.

Before we can design the optimization process, we need to formulate the robot's movement with equations and variables that will be used as the optimization parameters. Each biped walking gait cycle includes two walking steps, which have the same movement trajectories at each joint except that the legs swap their roles. The stance leg of the first walking step becomes swing leg in the second step.

Therefore, in order to reduce the number of optimization variables, we only need to consider one walking step when constructing the joint trajectories.

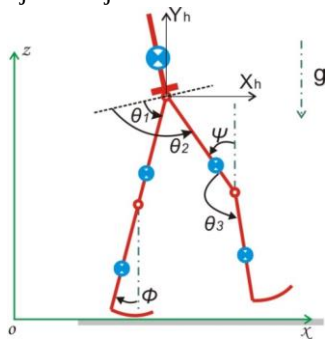

Fig. 3. The kinematics model of the robot used in simulation. The location of the center of mass of each link is indicated.

For fully actuated biped robots, the trajectories of all joints and the duration of a walking step can be arbitrarily chosen in a reasonable range. This is not the case of the passive-ankle walkers. Due to the un-actuated ankle, the trajectory of the stance leg and the duration of the walking step are determined by the natural dynamics of the robot, and can not be freely chosen. Below, we describe how the joint trajectories of the robot model are constructed in each of the stages of one walking step.

Single support stage

The single support stage starts immediately after the swing leg lands. As the knee of the stance leg is locked during this stage, total number of degrees of freedom is 4. The origin of the frame is set at the location where the previous swing heel touches the floor (see Fig.3). When the swing shank reaches the mechanical stop, a strike can occur if the speed is not zero. We will set a constraint in the trajectory planning to avoid this strike of the swing knee joint. With the Lagrange method, the equations that govern the motion of the simulated robot in its single-support stage are described as:

$$D(q)\ddot{q} + C(q,\dot{q}) + G(q) = \tau \qquad (1)$$

where $q = [\phi, \theta_1, \theta_2, \theta_3]^T$ is a vector describing the configuration of the robot (for definition of $\phi, \theta_1, \theta_2, \theta_3$, see Fig. 3), *D(q)* is a 4×4 inertia matrix, $C(q,\dot{q})$ is a 4×1 vector of centripetal and coriolis forces, *G(q)* is a 4 × 1 vector representing gravity forces, $\tau = [\tau_0, \tau_1, \tau_2, \tau_3]^T$, $\tau_0, \tau_1, \tau_2, \tau_3$ are the torques applied on the stance foot, the stance hip, the swing hip, and the swing knee joints, respectively (see Fig.3). Because the ankle is fixed and there is no actuator at foot, the torque around the ground contact point of the stance foot is zero ($\tau_0 = 0$). To separate the un-actuated joint from the actuated ones, let $\Theta = [\theta_1, \theta_2, \theta_3]^T$ represents the three actuated joints (see Fig.3).

Similar to [29] and many other optimization studies on biped walking robots, we use 2-knot cubic spline functions [22] to construct the trajectories of the three actuated joints, Θ.

$$\theta_i(t) = \begin{cases} a_3 t^3 + a_2 t^2 + a_1 t + a_0 & 0 \le t < T_m \\ b_3 (t - T_m)^3 + b_2 (t - T_m)^2 + b_1 (t - T_m) + b_0 & T_m \le t < T \end{cases} \qquad (2)$$

Where T is the duration of the walking step. $\boldsymbol{T_m = T/2}$, is the time for the intermediate configuration $\theta_i(T_m)$. In the hip joints (***i=1, 2***), this cubic spline function can be uniquely defined by specifying initial position and velocity ($\theta_i(0), \dot{\theta}_i(0)$), intermediate position and velocity ($\theta_i(T_m), \dot{\theta}_i(T_m)$), and final position and velocity ($\theta_i(T), \dot{\theta}_i(T)$). The final velocity of hip joints is zero.

During the single support stage, the knee joint of the swing leg (θ_3 in Fig.3) has two sub-phases, flexion and extension. Each of these sub-phases is described with a set of spline functions like in (2). Their time durations are T_e (for extension) and T_f (for flexion), respectively. Of course, $T_e + T_f = T$. The initial and final position of the swing knee joint, $\theta_3(0)$ and $\theta_3(T)$, are set at zero, because the leg is straight at the beginning and the end of the walking step. To avoid the knee strike, we also have, $\dot{\theta}_3(0) = \dot{\theta}_3(T) = 0$. The final state of the flexion phase, $\theta_{3,f}(T_f)$ and $\dot{\theta}_{3,f}(T_f)$, and the initial state of the extension phase, $\theta_{3,e}(0)$ and $\dot{\theta}_{3,e}(0)$, are the same. $\dot{\theta}_{3,f}(T_f)$ is 0. The intermediate states of the flexion phase ($\theta_{3,f}(T_f/2)$ and $\dot{\theta}_{3,f}(T_f/2)$) and the extension phase ($\theta_{3,e}(T_e/2)$ and $\dot{\theta}_{3,e}(T_e/2)$)will be the optimization parameters.

Once $\Theta(t)$ is constructed as in (2), the evolution of the un-actuated ankle joint, ϕ, can be computed by integrating the first equation of equation (1), which can be re-written as,

$$D_1(\phi, \Theta)\ddot{\phi} + C_1(\phi, \Theta, \dot{\phi}, \dot{\Theta}) + G_1(\phi, \Theta) = 0 \qquad (3)$$

Where D_1, C_1, and G_1 are the first row of D, C, and G in equation (1), respectively.

Due to the relatively heavy torso, the two hip joints are coupled severely to each other, and thus higher PD gains are used in robot experiments at hip motors. However, as the gains in the real robot system are limited by the maximum torque of the motors, the real robot joints can not perfectly track the planned trajectories as in the simulation. This is part of the reason for the discrepancy between the real robot experimental results and the simulation results.

After ***q*** is defined or computed by using equation (2) and (3), the ground reaction forces can be computed using the acceleration of the centre of mass of the robot. The position of the centre of mass of the robot can be formulated as a function of ***q*** (see Fig.3):

$$\begin{bmatrix} x_c \\ z_c \end{bmatrix} = \begin{bmatrix} f_x(q) \\ f_z(q) \end{bmatrix} \qquad (4)$$

Thus, the ground reaction forces at the ***x*** and ***z*** axis can be calculated as:

$$\begin{bmatrix} F_x \\ F_z \end{bmatrix} = m \begin{bmatrix} \ddot{x}_c \\ \ddot{x}_z \end{bmatrix} + mg \begin{bmatrix} 0 \\ 1 \end{bmatrix} \qquad (5)$$

where m is the total mass of the robot.

Landing stage

At time t=T, the swinging foot lands and the transient landing stage starts. During this stage, the configuration of the robot, ***q,*** doesn't change. The strike of the swing heel is assumed to be an inelastic impact. This assumption implies the conservation of angular momentum of the robot just before and after the strikes. Thus the value of $\dot{q}$ just after the strikes

, $(\dot{q}^+)$, can be computed using its value just before the strikes,

$\dot{q}^-$. So, we have,

$$\dot{q}^+ = H(q^-, \dot{q}^-) \quad (6)$$

Where $q^- = [\phi(T), \Theta(T)]^T$, and $\dot{q}^- = [\dot{\phi}(T), \dot{\Theta}(T)]^T$. $\phi(T)$ can be calculated with $\Theta(T)$, because at time t= T, both leg are straight and touch the floor.

Just after the landing of the swing foot, the two legs swap their roles. As described above, $[q(0), \dot{q}(0)]^T$ is the initial state of the robot when current walking step starts, and $[q^+, \dot{q}^+]^T$ is the initial state of the next walking step. Because the walking gait is cyclic, we have the following cyclic constraint:

$$\begin{bmatrix} q(0) \\ \dot{q}(0) \end{bmatrix} = E \begin{bmatrix} q^+ \\ \dot{q}^+ \end{bmatrix} \quad (7)$$

Where E is a matrix representing the role-swapping of the two legs.

B. *Process of optimization*

As described above in IIIA, using equations (1)—(7), the evolution of the robot state during one walking step is completely defined by the parameters in Table 1.

Table 1. The optimization parameters

Duration of the single support stage	T
Duration of the flexion phase of swing knee	T_f
Final position of hip joints	$\theta_i(T)$, *i=1, 2*
Intermediate state of hip joints	$\theta_i(T_m), \dot{\theta}_i(T_m)$ *i=1,2*
Intermediate state of flexion phase in swing knee	$\theta_{3,f}(T_f/2)\ \dot{\theta}_{3,f}(T_f/2)$
Intermediate state of extension phase in swing knee	$\theta_{3,e}(T_e/2)\ \dot{\theta}_{3,e}(T_e/2)$
Final position of the flexion phase in swing knee	$\theta_{3,f}(T_f)$
Final velocity of the un-actuated ankle joint	$\phi(T)$

But, how to select the values of these parameters in Table 1 to generate fast and stable walking patterns? We formulate this as a constrained nonlinear optimization problem: find the values of the parameters in Table 1 that maximize the walking speed:

$$J = \frac{x(T)}{T} \quad (9)$$

Where ***x(T)*** is the position of the swing foot at time ***t = T***. The optimization problem is solved numerically using the ***fmincon*** function in Matlab. It uses a Sequential Quadratic Programming (SQP) method to find the optimum of the cost function in equation (9) under the several nonlinear constraints (e.g., maximal torque/speed, step-length) and a stability criterion. In each iteration, estimated values of the optimization parameters listed in Table 1 are used to compute the trajectories of the robot according to equations (1)-(3), and thus getting the estimation of the optimization parameters for the next iteration. When the algorithm converges, the optimal values of the optimization parameters are found.

The optimization process is run repeatedly with different step-angles (step-length). Firstly, to get walking patterns with upright-torso, we run the optimization process with a further constraint: during the walking step, the angle between the torso and the vertical line must be lower than 2 degree. Secondly, to get the swaying-torso walking patterns, we remove this constraint and re-run the optimization process.

IV. RESULTS OF THE OPTIMIZATION

A. *Fast walking patterns obtained in optimization*

The result of the optimization process is shown in Fig.5. The range of the step-length that can generate stable walking patterns in the swaying-torso walking is much larger than in the upright-torso walking (see Fig.5). The fastest speed of the swaying-torso walking is 40% higher than that of the upright-torso walking (see Fig.5). To show more features of the fast walking patterns with and without torso-swaying, we look at the following three typical walking patterns:

(1) The fastest walking with swaying-torso (point a in Fig.5).
(2) The fastest walking with upright-torso (point b in Fig.5).
(3) The fastest walking with upright-torso and largest allowable step-length (point c in Fig.5).

The stick diagram and the instantaneous speeds of the mass centre of torso in these three walking patterns are shown in Fig. 6.

As revealed in Fig.5 and Fig.6B, the strategy for fast walking with upright-torso is to have a smaller step-length (see Fig.5) but high step-frequency (see Fig.6B). This is consistent with the results of our previous study on another biped robot [7]. For comparison, some key features of the

Table 2. Features of the three typical walking patterns

Walking pattern	Stride-length (cm)	Stride-frequency (Hz)	Overall walking speed (cm/s)	Fluctuation range of instant speed (%)
Swaying torso, fastest walking. Fig.4(a) Fig.5A	**18.0**	**4.3**	**78.2**	**24** *(see Fig.4(a))*
Upright torso, fastest walking. Fig.4(b) Fig.5B	**12.7**	**4.4**	**55.7**	**18** *(see Fig.4(b))*
Upright torso, largest stride. Fig.4(c) Fig.5C	**16.5**	**1.8**	**30.4**	**67** *(see Fig.4(c))*

three walking patterns are also listed in Table 2. As shown in Table 1 and Fig.6, the step-frequency of the fastest swaying-torso walking is nearly as high as that of the fastest upright-torso walking. But its step-length is much larger (see Table 2). This is the reason that the swaying-torso walking is faster.

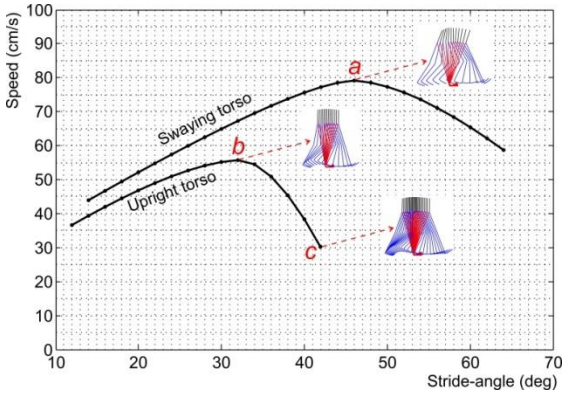

Fig.5 The fastest walking speeds got from the optimization process (see fig.4) at different step-angle. Three typical walking patterns corresponding to the point a, b, and c are also shown. For detailed comparison of these walking patterns, see the text and Fig.6.

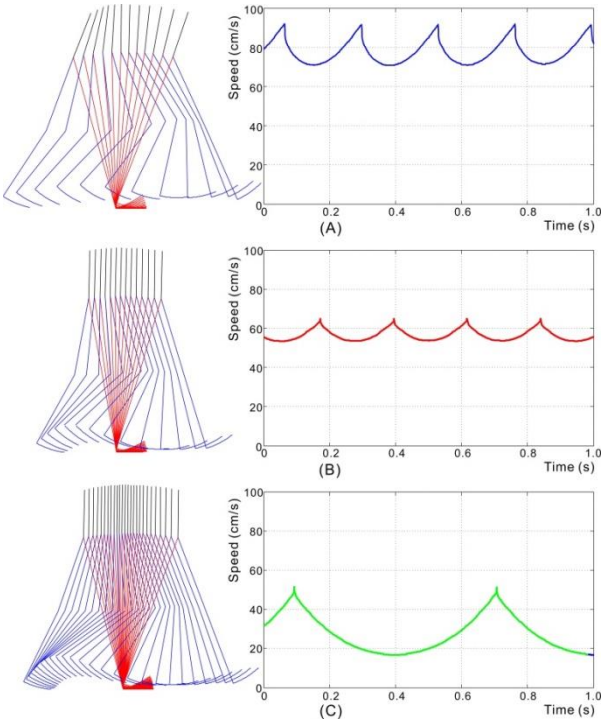

Fig. 6 Stick-diagrams and instantaneous walking speeds of the three typical walking patterns: (A) fastest swaying-torso walking (point a in Fig.5); (B) fastest upright-torso walking (point b in Fig.5); (C) upright-torso walking with the largest step-length (point c in Fig.5).

V. Prototype Experiments

The optimal trajectories with swaying or upright torso and various step-lengths (i.e., the points in Fig.5) are applied on the real robot under its controller. If the robot can walk for one round in the arena without falling (see Fig.2), the walking pattern is regarded as stable. The overall walking speed of the robot is estimated simply by measuring how long it takes for the robot to walk one round in the arena (see Fig. 2). As shown in Fig.10, the range of step-lengths that can have stable walking in the real robot is smaller than in the simulated robot. Moreover, the walking speed of the real robot is higher than that of the simulated one. Despite these discrepancies, the relationship between the speed and the step-length in the real robot has the same trend as in the simulated one (see Fig.10). For example, the fastest walking patterns have a large step-length with swaying-torso (point a in Fig.10), and small step-length with upright-torso (point b in Fig.10).

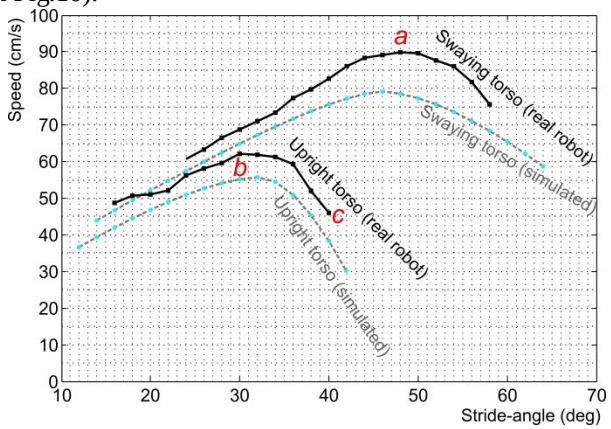

Fig. 10 The black lines are the walking speed of the stable swaying-torso walking and upright-torso walking with various step-lengths (step-angle here) in the real robot. For comparison, the walking speed curves of the simulated robot shown in Fig.4 are also put here in blue color.

Snapshots of the fastest walking gait with swaying-torso are in Fig. 13. It shows the rhythmic sway of the torso during a walking step. For legged robots, a video may tell much more than the data could. Please watch a video footage of the fastest swaying-torso walking at,
https://sites.google.com/site/dadatwtw/Home/FASTBIPED.avi?attredirects=0&d=1

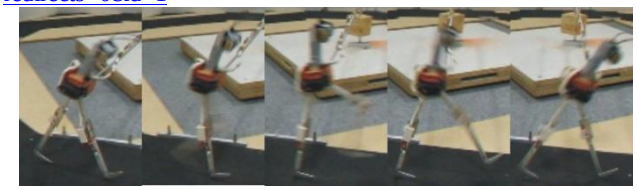

Fig. 13 A series of snapshots of the fastest walking with swaying-torso.

VI. Conclusion and Discussion

The torso's effects on various aspects of biped walking have been studied in the literature. This study was started with an intuitive hypothesis: Rhythmic sway of torso might enable faster walking in under-actuated bipeds. Firstly, we have simulated a passive-ankle walker model and analyzed how the optimized swaying movements of torso affect its walking speed and robustness. Then we applied the optimal trajectories on a real robot. Despite the reality gap between the simulation and the real robot's experimental results, both of them indicated that the optimized torso-swaying can greatly increase the walking speed of passive-ankle walkers. Our analysis of the simulation results and the experimental

data also revealed the reason for the fast walking with swaying-torso: The rhythmic sway of torso mitigates the braking-and-accelerating effect of large-step walking in PAWs, thus enabling the robot to walk with a relatively large step-length while still keeping a high step-frequency.

REFERENCES

[1] V. T. Inman, H. J. Ralston, F. Todd, *Human Walking*, Williams & Wilkins, 1981

[2] A. Eredmir, S.J. Piazza, "Rotational foot placement specifies the lever arm of the ground reaction force during the push-off phase of walking initiation," *Gait and Posture*, vol. 15, no. 2, pp. 212-219, 2005.

[3] D.G.E. Hobbelen and M. Wisse, "Ankle Actuation for Limit Cycle Walkers," *Int. J. Robotics Research*, vol. 27, no. 6, pp. 709-735, 2008.

[4] J. Dean, A. Kuo, "Elastic coupling of limb joints enables faster bipedal walking," *J. Royal Society Interface*, vol. 6, no. 16, pp. 561–573, 2009.

[5] C. Chevallereau, G. Abba, Y. Aoustin, F. Plestan, E. Westervelt, C. Canudas-deWit, and J. Grizzle, "Rabbit: A testbed for advanced control theory," *IEEE Control Systems*, vol. 23, no. 2, pp. 57-79, 2003.

[6] K. Sreenath, H. Park, I. Poulakakis, and J. W. Grizzle, "Compliant hybrid zero dynamics controller for achieving stable, efficient and fast bipedal walking on MABEL," *Int. J. Robotics Research*, vol. 30, no. 9.

[7] T. Geng, B. Porr, and F. Wörgötter, "Fast biped walking with a sensor-driven neuronal controller and real-time online learning," *Int. J. Robotics Research*, vol. 25, no. 3

[8] http://www.youtube.com/watch?feature=player_detailpage&v=VbwArcacW6g

[9] T. Geng, & J. Q. Gan, "Planar biped walking with an equilibrium point controller and state machines," *IEEE/ASME Trans. Mechatronics*, vol. 15, no. 2, 2010.

[10] J. Pratt, *Exploiting Inherent Robustness and Natural Dynamics in the Control of Bipedal Walking Robots*, Massachusetts Institute of Technology, 2000

[11] M. Chen, "Analysis and control techniques for the compass gait with a torso walking on stochastically rough terrain," In *American Control Conference*, 2012.

[12] F.B. Ouezdou, B. Mohamed, V. Scesa, R. Sellaouti, "Design and experiments of a torso mechanism for the ROBIAN biped robot," *Robotica*, vol. 24, no. 3.

[13] P. R. Vundavilli, S. K. Sahu, "Dynamically balanced ascending and descending gaits of a two-legged robot," *Int. J. Humanoid Robotics*, 2006.

[14] J. Zhao, et al. "Optimized Configuration for the Upper Body with a Bisecting Hip Mechanism in Passive Dynamic Walking," *Applied Mechanics and Materials*, vol. 39, pp. 306-311,2011.

[15] F. Asano, and Z.W. Luo. "Underactuated virtual passive dynamic walking with an upper body," in *Proc. IEEE Conf. Robotics and Automation*, 2008, pp. 2441-2446.

[16] M. Takahashi, T. Narukawa, K. Miyakawa and K. Yoshida. "Combined control of CPG and torso attitude control for biped locomotion," in *Proc. IEEE/RSJ Conf. Intelligent Robots and Systems*, 2005.

[17] R. Dehghani, and A. Fattah. "Motion control and efficiency analysis of a special design five-link biped robot with torso," in *Proc. IEEE/ASME Int. Conf. Mechtronic and Embedded Systems and Applications*, 2008, pp. 198-203.

[18] B. Ugurlu, J. A. Saglia, N. G. Tsagarakis, & D. G. Caldwell, "Yaw moment compensation for bipedal Robots via Intrinsic angular momentum Constraint," *Int. J. Humanoid Robotics*, vol. 9, no. 4, 2012.

[19] Y. Kang, J. Park and H. Yim, "Walking Pattern Generation for a Biped Robot using Optimized Polynomial Approximation," in *Proc. IEEE-RAS/RSJ Int. Conf. Humanoid Robots*, 2004.

[20] H. Dallali, M. Brown, B. Vanderborght, "Using the Torso to Compensate for Non-Minimum Phase Behaviour in ZMP Bipedal Walking," *Advances in Robotics Research*, vol.6, pp. 191–202, 2009.

[21] K. Kappaganthu, & C. Nataraj, "A Biped With a Moving Torso," *Int. J. Humanoid Robotics*, 2009.

[22] J.H. Ahlberg, E.N. Nilson, J.L. Walsh, *The Theory of Splines and Their Applications*. Academic Press, New York, 1967.

[23] T. Geng, B. Porr, and F. Wörgötter, "A Reflexive Neural Network for Dynamic Biped Walking Control," *Neural Computation*, vol. 18, no. 5. 2006.

[24] J. Godowski, S. Cotton, I. Olaru and J. Pratt, "Comparing Performance of Running Robots: Gravity, Size, Speed and Stride as Metrics for Dynamic Performance," *Dynamic Walking*, 2012.

[25] E. R. Westervelt, B. Gabriel, and J. W. Grizzle. Experimental validation of a framework for the design of controllers that induce stable walking in planar bipeds. *Int. J. Robotics Research*, 2004.

[26] T. McGeer, "Passive dynamic walking," *Int. J. Robotics Research*, vol. 9, no. 2, pp. 62-82, 1990.

[27] M W,Spong, J K, Holm, D. Lee, "Passivity-based control of bipedal locomotion," *IEEE Robotics & Automation Magazine*, vol. 14, no. 2, pp. 30-40, 2007.

[28] A. L. Schwab and M. Wisse, "Basin of attraction of the simplest walking model," in *Proc. ASME Int. Conf. Noise and Vibration.* 2001, Pennsylvania.

[29] D. Tlalolini, C. Chevallereau, Y. Aoustin, Human-Like Walking: Optimal Motion of a Bipedal Robot With Toe-Rotation Motion," *IEEE/ASME Trans. Mechatronics*, vol. 16, pp. 310-320, 2011.

[30] S. Lee, and J. P. Stephen. "Built for speed: musculoskeletal structure and sprinting ability," *J. Experimental Biology*, vol. 212, no. 22, pp. 3700-3707.

[31] R. Alexander and A. Jayes, "A dynamic similarity hypothesis for the gaits of quadrupedal mammals," *J. Zoology*, vol. 201, pp. 135-152, 1983.

[32] C. Chevallereau and Y. Aoustin, "Optimal reference trajectories for walking and running of a biped robot," *Robotica*, vol. 19, no. 5, pp. 557–569, 2001.

[33] T. Geng, "Torso-inclination Enables Faster Walking in A Planar Biped Robot with Passive Ankles", *IEEE transactions on Robotics*, Vol. 30, No. 3, 2014, pp 753-758.